BIW10 Preprint -- Edited; preliminary green dot status
Final version will appear on JACoW

INJECTION BEAM DYNAMICS IN SPEAR3*

J. Corbett[1], W. Cheng[2], A.S. Fisher[1], X. Huang[1], W. Mok[3], J. Safranek[1] and S. Westerman[1]
[1]SLAC National Accelerator Laboratory, Menlo Park, CA 94025
[2]Brookhaven National Laboratory, Upton, NY 11973
[3]Life Imaging Technology, Palo Alto, CA 94301

Abstract

For the top-off operation it is important to understand the time evolution of charge injected into the storage ring. The large-amplitude horizontal oscillation quickly filaments and decoheres, and in some cases exhibits non-linear x-y coupling before damping to the stored orbit. Similarly, in the longitudinal dimension, any mismatch in beam arrival time, beam energy or phase-space results in damped, non-linear synchrotron oscillations. In this paper we report on measurements of injection beam dynamics in the transverse and longitudinal planes using turn-by-turn BPMs, a fast-gated, image-intensified CCD camera and a Hamamatsu C5680 streak camera.

INTRODUCTION

SPEAR3 is a 3rd generation, 3GeV storage ring light source with nominal emittance ε_x=10nm-radian. Single-bunch top-off injection occurs at either 8 hr or 10 min intervals with photon beamline shutters open [1]. Since the injector and BTS transport line were not specifically designed for top-off, it is particularly important to measure and understand dynamics of the injected beam in order to minimize perturbations seen by the users and to protect sensitive ID magnets in the lattice.

The injection system consists of a 10Hz booster synchrotron with single-bunch filling capability. Under nominal I=200mA operating conditions each stored bunch contains ~550pC (700uA) and each injected pulse contains ~30pC (40uA). The contrast makes measurement of the injected pulse difficult. A vertically-deflecting Lambertson septum brings the beam to SPEAR3 with the injected beam at x=-13mm. Several key parameters related to injection are listed in Table 1.

A number of diagnostic instruments are used to measure the injected beam dynamics. Centroid motion is monitored with fast turn-by-turn BPMs developed specifically for SPEAR3 [2]. Optical imaging of the charge distribution is possible at a diagnostic beam line which directs 3.5 x 6mrad of unfocused visible/UV light to an optical bench. After passing through a 6" diameter, f=2m collection lens the light is relayed to one of several diagnostic stations. An intensified, fast-gated camera can image the transverse beam profile at each turn [3] but the light intensity is low and in most cases must be averaged over consecutive injection events [4]. Similarly, in the longitudinal direction, a dual-axis streak camera can be used to image the injected beam profile by integrating over a series of injection pulses [5]. For a detailed analysis of the transient response of the injected beam into a storage ring see references [6,7].

*Work sponsored by U.S. Department of Energy Contract DE-AC03-76SF00515 and Office of Basic Energy Sciences.
[1]corbett@slac.stanford.edu

Table 1: SPEAR3 injection parameters

Injection amplitude	x=-13 mm
Stored beam size	310x20 μm, 20 ps
Stored beam, dp/p	0.1%
Damping times	4.2, 5.1, 2.8 ms
Injected beam size	~1.0x0.8 mm at SLM
Injected dp/p	0.07%

BTS TUNING AND TURN-BY-TURN BPMS

As reported in [8], a systematic program was carried out to optimize electron beam steering and lattice optics through the booster-to-SPEAR (BTS) transport line. Important elements of this work included removal of stainless steel windows intercepting the beam path and application of response-matrix analysis to correct the beam optics.

The injection kicker waveforms were then carefully matched and 6-D phase-space coordinates of the incoming beam adjusted by monitoring the bunch centroid motion on turn-by-turn BPMs. For these measurements, specially-designed Ecotek BPM receivers [2] mix the raw BPM signals down to an intermediate frequency $f_{IF} = 13f_0$ that is band-pass filtered and allowed to electronically ring several times while being digitized by high quality commercial digitizers. In order to monitor and compensate for changes in gain, a low-level calibration signal at $f_{cal} = f_{RF} - f_0/2$, is combined into the BPM long haul cables. Parallel digital receivers tuned to both f_{RF} and f_{cal} respectively allow for the calibration. The resulting digitally-processed data yields low-distortion, highly-accurate measurements of beam position on a turn-by-turn basis. For nominal stored-beam conditions the beam centroid resolution is of order 1μm.

For injected-beam measurements, the incoming single-bunch charge is only ~30pC so the BPM signals are relatively weak, -85dBm after cable loss, and the position resolution is only about 1mm. As a result, horizontal injection oscillations can be resolved but small amplitude vertical motion and synchrotron oscillations require averaging. In order to measure individual injection pulses, at each injection cycle injection kicker #3 (downstream of the injection septum) is triggered at the nominal injection time while injection kickers #1 and #2 (upstream of the septum) are mismatched and triggered 50ms late to kick out the stored beam [8].

Of particular interest, the synchrotron oscillation component was extracted via FFT processing and the initial phase-space coordinates of the motion used to match injected beam energy and timing. An example

where the injection beam is phase mismatched is illustrated in Fig. 1. In this case the synchrotron

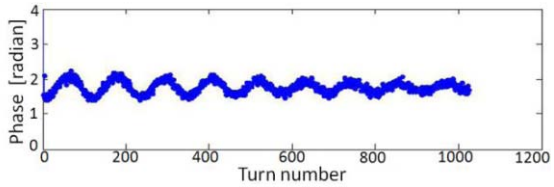

Figure 1: Synchrotron oscillations on the beam centroid due to booster/SPEAR timing mismatch.

oscillation amplitude is large, about 1 radian in rf phase. At 781ns per turn, the ~125 oscillation period agrees well with the nominal 10kHz synchrotron oscillation frequency. Although the beam arrival time can be adjusted manually, the phase drift typically requires adjustment several times per day. The source of error lies in temperature variation of the long-haul cable connecting the 476MHz SPEAR3 master oscillator to the 358MHz booster master oscillator. Various ways to automatically correct the phase error are being investigated including installation of a transmission line interferometer and direct measurement of the low-amplitude synchrotron oscillations on the injected pulse in the presence of stored beam. Once the injected beam energy has been optimized it typically remains stable over the course of several months [8].

TRANSVERSE BEAM DYNAMICS

A fast-gated, MCP-intensified PiMax camera was used to image the transverse profile of the beam at injection. Visible light focused through a commercial 1:5 lens onto the front-end photocathode yields a net de-magnification of M=0.59. A parallel optical path uses a combination of single-plane cylindrical lenses to yield a net de-magnification of M_x=0.7 and M_y=0.2 in the x/y planes, respectively [4,9]. In both cases the SR light passes through a vertical corner-periscope to create a 90 degree coordinate rotation. The horizontal beam axis and horizontal betatron motion are then oriented perpendicular to the optical bench and along the vertical axis of the camera CCD.

With the cylindrical lens system, the beam image has a tall, narrow orientation so that a fast, rotating mirror can sweep the image horizontally across the face of the camera. A series of spatially separated images can then be acquired in a single CCD exposure [9]. An example of data taken with the rotating mirror is illustrated in Figure 2. In this case a single stored-bunch is subject to an impulsive horizontal kick and beam distribution is imaged for all turns over the 10ms interval of mirror rotation. The betatron damping time agrees well with calculations and turn-by-turn BPM measurements. The rotated image of a single-pass to the right in Fig. 2 shows the effect of charge filamentation in phase space at t=120μs.

In principle single-bunch imaging within a full bunch train is possible using the 2ns photocathode gate but the

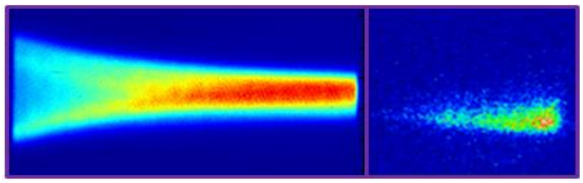

Figure 2: Damped horizontal betatron oscillation of stored beam, 10ms exposure & single turn at t=120μs.

images suffer from bleed-through of photons radiated by the rest of the beam. The camera gate extinction ratio is 10^6 [3], so a 3ms mechanical shutter is required to reject light arriving before and after the exposure to achieve clear images with ~10^8 extinction ratio.

Similar to the BPM system, turn-by-turn imaging of the injected beam is complicated by low signal levels. In this case, with all filters removed, each turn yields a few thousand photons per pass across the UV/visible camera detection bandwidth [10]. When the electron beam is well focused, light from a single injection pulse on a single turn can be amplified by the MCP to yield only a feint image even under darkroom conditions. As the beam filaments the photon flux is spread out over more pixels and the image becomes increasingly difficult to detect.

To enhance contrast, the PiMax software is configured to take multiple exposures of a single turn over a series of injection pulses. Starting from a t=-320μs pre-trigger pulse, light from ten's of separate injection events is integrated on the CCD chip to produce a single camera 'frame' before readout and advance to the next frame. The software *sequence* mode is used to set the frame exposure count and advance from turn-to-turn as the booster injects beam into SPEAR3. As described above, the charge from each injected pulse is ejected using mis-timed kickers prior to the next injection cycle.

Figure 3 shows an example of the multi-exposure,

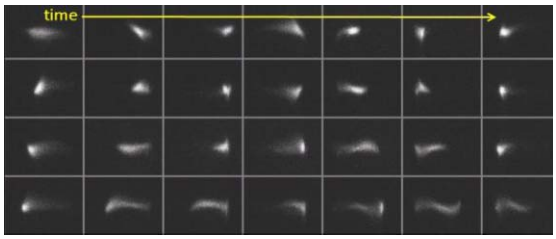

Figure 3: Transverse images of injected beam on consecutive turns. Coordinate rotations corrected.

multi-turn imaging technique utilizing the 1:5 lens branch line (no rotating mirror). The left/right motion is due to the inherent horizontal betatron oscillation in the injected beam and up/down motion indicates some degree of coupling. Each image represents a transverse projection of the charge distribution on consecutive turns. At the extremes in horizontal position the charge distribution appears as a relatively tight spot while exposures taken as the charge passes across the center of the screen generate 'comet-like' images. As sketched in Fig. 4, one plausible

explanation is that tune shift with betatron amplitude leads to charge filamentation. Other possible causes include chromaticity with energy spread and tumbling of a mismatched beam as it rotates in phase-space. Either way, the camera only sees images projected onto the x-axis from the full x-x' phase space distribution.

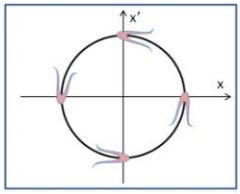

Figure 4:Charge filamentation in x-x' phase-space.

In a more complete scenario each image can be viewed as an x-y projection of the 3-D bunch structure or 'snake' of injected charge moving toward the observer. A full account of the transverse turn-by-turn images must then take into account evolution of the vertical and longitudinal charge distribution in time. The potential to image the beam in the x-t and y-t planes and thereby resolve the full snake-like 3-D charge distribution is discussed in the next section.

One consequence of charge filamentation is the appearance of rapid damping of the beam centroid as seen by the BPMs. Hence, as illustrated in Fig. 5, the nominal 3500-turn damping time can be masked by non-linear filamentation of the injected charge.

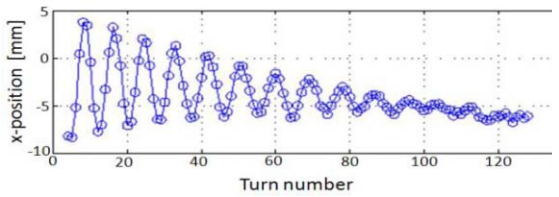

Figure 5: BPM measurement of the injected beam centroid in the horizontal plane.

Interestingly, the pulse-to-pulse beam dynamics, although complicated, is reproducible. The image of turn #28 shown in Fig. 6(a) was reproduced over many independent measurements despite the strong x/y coupling. In this case, it is likely the bunch has 3-D structure directed perpendicular to the page. In Fig. 6(b), a high-field wiggler field is removed and the same turn #28 demonstrates a different, reproducible distribution. Figure 6(c) shows yet another example of turn #28 when the SPEAR3 lattice is adjusted to low-alpha optics. Clearly the dynamical evolution of the injected charge distribution is a complicated function of subtle changes in the magnetic field distribution within the storage ring.

Further into the injection process, the charge distribution continues to smear in the x-y plane until the photon flux density becomes so low that details are difficult to resolve. The time sequence displayed in Fig. 7 shows how after a several damping times, the injected charge re-coalesces to the closed-orbit beam axis. Here, starting at t=100μs, the time evolution of injected charge is captured every 2ms, and the rf voltage was lowered to

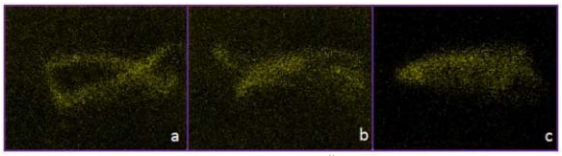

Figure 6: Comparison of turn #28 for three different magnetic lattice configurations

the level where only a few μA of charge remains to mark the stored beam axis but does not accumulate. For each exposure the camera gate was held open for 5μs. Although the charge couples into the vertical plane the injected charge capture efficiency is known to approach 100% under optimal injection conditions.

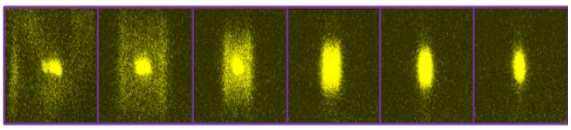

Figure 7: Injected charge distribution every 2ms.

LONGITUDINAL BEAM DYNAMICS

In terms of longitudinal coordinates, the injected beam is captured and damped in the non-linear potential of the rf system. Ideally the injected charge is matched in arrival time (synchronous phase), distribution in arrival time, average beam energy and energy spread. This section investigates injected beam dynamics in the longitudinal plane for long- and short timescales. In each case the Hamamatsu C5680 streak camera is used to collect data in dual-scan mode. By way of review, the streak camera reveals the longitudinal beam profile along the fast, vertical camera axis while the slower horizontal axis captures the evolution of time-dependent beam dynamics.

Since precise measurements of bunch length are not required here and the radiated light intensity is often low, no optical filters or color attenuators are used. For low intensity measurements the signal is integrated on the camera CCD using the inject/kickout scheme described above. The vertical time scale for the R2 synchroscan is 704ps full scale or 0.69ps-per-pixel.

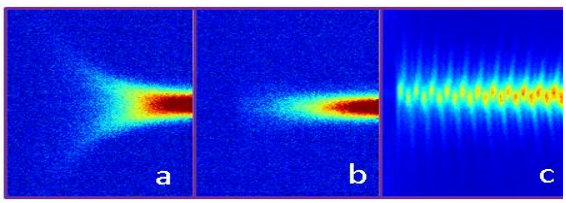

Figure 8: Dual-scan streak camera image of injected beam on 10ms and 1ms time scales.

Starting with long time scale injection phenomena, Fig. 8 shows beam capture during the first 10ms of beam capture with (a) injection phase mismatch and (b) correct timing during the first 10ms of injection ($\tau_{||,damp}$=2.8ms). The initial large-amplitude oscillations are not visible with correct timing. Figure 8(c) zooms in to the 1ms time

scale to illustrate the presence of 10kHz synchrotron oscillations, even with accurate injection timing.

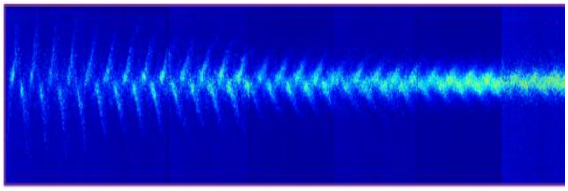

Figure 9: Evolution of longitudinal bunch distribution during first 3.5ms after injection.

Figure 9 shows the same injected charge sequence during the first 3.5ms, in this case rendered from a series of seven 500μs horizontal-sweep images stacked together in software. Similar to motion in the transverse plane, time evolution of the bunch in the longitudinal dimension can be influenced by filamentation and/or tumbling of the bunch in phase-space. In this case filamentation is caused by synchrotron tune shift with amplitude in the non-linear rf potential. The motion, however, maintains a relatively coherent structure as charge damps to the synchronous phase. In the damped condition the stored beam typically executes ~1ps rms coherent synchrotron oscillations.

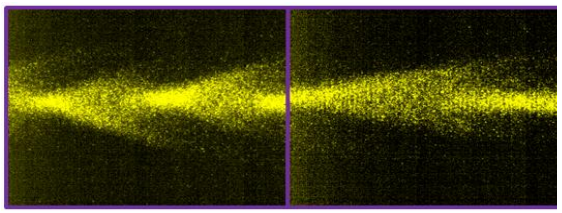

Figure 10: Evolution of injected charge distribution on 100μs and 50μs time scales at t=1.27ms.

Moving to later-time injection dynamics, Fig. 10 shows evolution of the charge distribution on the 100 μs and 50μs time scales after 1.27ms into the process. The tails observed in the images can be correlated with a highly-filamented time/energy phase-space structure projected to the time axis [11].

If we now zoom in to short-time dynamics, Fig. 11(a) shows clear evidence of phase-space mismatch in the injected beam. The projected charge density as seen by the streak camera periodically appears as a 'condensed' image and a 'diffuse' image alternating at twice the synchrotron frequency as the distribution rotates in phase-space. In the 'diffuse' projection the bunch length is found to be several hundred ps long. The corresponding energy spread can be extracted from the 'condensed' state. A good description of these phenomena with a comparison to simulation is given in [11].

In Fig. 11(b) the horizontal time scale is further reduced to 50μs so that initially the injected bunch can be resolved on a turn-by-turn basis in 2-D x-t coordinates. The small tilt or x-t correlation is indicative of charge dispersion in the horizontal plane as seen on the PiMax camera. After about 10 turns, a more complete de-coherence is evident.

Of note, the images in Fig. 11 were integrated over 30 injection pulses, again demonstrating a high level of injector stability over short time intervals. This is consistent with the turn-by-turn PiMax data shown above.

In order to further resolve turn-by-turn beam dynamics the optical beam transport line leading to the streak camera was modified to incorporate cylindrical lenses. The nominal streak camera configuration utilizes a Leice Acro 10/0.25 objective lens to produce a small focus at the entrance the slit of the streak camera. In the cylindrical lens configuration, a weak horizontal lens was used in conjunction with a strong vertical lens to produce

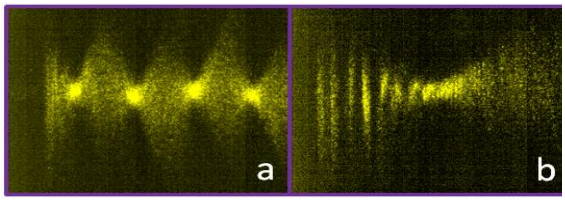

Figure 11: Evolution of charge injected bunch distribution on (a) 200μs and (b) 50μs time scales.

magnification in the horizontal direction and de-magnification in the vertical direction. The small vertical spot size is necessary for good time resolution.

The camera is then operated with a 500ns horizontal time base to capture single turns during injection. Similarly, by rotating the incoming beam with a dove prism, the bunch can be imaged in the y-t plane. In conjunction with the PiMax camera, the object was to capture a full rendering of the injected bunch in x-y-t coordinates. Unfortunately the initial results were ambiguous, in part because the horizontal magnification was too high and in part because the large amplitude betatron motion is hard to capture a turn-by-turn basis.

Variable RF Voltage

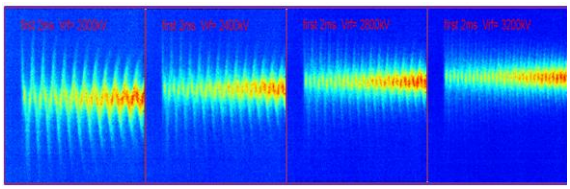

Figure 12: Variation of injection oscillations with increasing rf voltage (2.0, 2.4, 2.8 and 3.2MV).

Since the injected bunch is captured in the potential of the rf system, it is interesting to investigate time evolution of the injected beam dynamics with variable rf voltage. The effect is shown in Fig. 12 where the rf voltage is increased from 2.0MV to 3.2MV in steps of 400kV. Under matched timing conditions, the charge distribution is seen to extend from about +/-200ps in the low-voltage case to only about +/-50ps in the high-voltage case. As expected the synchrotron oscillation frequency and synchronous phase scale with $\sqrt{V_{rf}}$.

Injection Timing Errors

By adjusting the injected beam arrival time, one can see the longitudinal beam dynamics with timing mismatch, as shown in Fig. 13. In first four plots to the left the horizontal sweep time is 1ms, vertical synchroscan range is R2 (704ps) and the delay times are 0, 20, 30 and 45ps relative to synchronous injection. From these images it is clear that filamentation and/or phase-space mismatch cause the charge to disperse over a range of time much greater than the bunch centroid delay time. The motion shown furthest to the right was taken in R4 synchroscan mode has 150ps injection delay. In this case the vertical time scale is 1687ps and the injected bunch exhibits coherent dipole-mode oscillations.

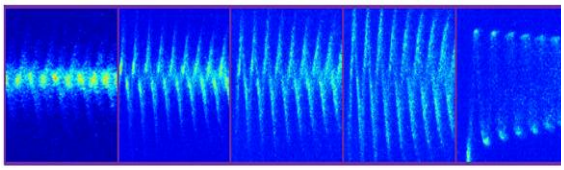

Figure 13: Longitudinal injection oscillations with arrival time error Δt=0, 20, 30, 45 and 150ps (R4).

SUMMARY

SPEAR3 is presently moving toward top-off operation at 10 min injection intervals. The incident charge must be well matched in the transverse and longitudinal dimensions for efficient capture, radiological concerns and ID protection. Turn-by-turn BPMs are used to control the 6-D launch conditions into the storage ring. Synchrotron light diagnostics are used to monitor different projections of the charge distribution. The fast-gated camera shows evidence of filamentation in the horizontal plane caused by tune shift with betatron amplitude and/or optical mismatch. In the longitudinal plane the correct timing, beam energy and phase-space distribution are needed to minimize turbulence in the rf bucket. Future studies will concentrate on reconstruction of the 3-D structure of the inject pulse at early times to understand and improve matching conditions.

ACKNOWLEDGEMENTS

We gratefully acknowledge the advice and assistance of Bill Cieslik, the SPEAR3 operations staff and the SLAC radiation physics department.

REFERENCES

[1] J. Schmerge, et al, “Summary Report on SPEAR3 top-off injection safety”, SSRL-AP-007, 2009.
[2] J. Sebek, “BPM system electronics design”, SSRL-ENG-NOTE M594, and J. Sebek, *et al*, “Design and performance of SSRL beam position electronics”, these proceedings.
[3] Roper Scientific, PiMax Camera, UV enhanced, www.princetoninstruments.com.
[4] W. Cheng, et al, “Fast-gated camera measurements in SPEAR3”, PAC09, Vancouver, Canada, 2009.
[5] W.Cheng, A.S.Fisher and J.Corbett, “Streak camera measurements in PEP-II and variable optics in SPEAR3”, BIW08, Lake Tahoe, CA (2008).
[6] H. Moshammer, ‘Transient response of the beam after injection in a storage ring”, NIMA 323, (1992).
[7] H. Moshammer, “Moments and characteristic function of a nonstationary particle distribution after injection”, Phys. Rev. E, Vol. 48, 3 (1993).
[8] J. Safranek, *et al*, “Optimization of the booster to SPEAR3 transport line for top-off injection”, PAC09, Vancouver Canada, 4-8 May, 2009.
[9] A.S. Fisher *et al.*, “Turn-by-turn imaging of the transverse beam profile in PEP-II”, BIW06, Batavia, IL, 1–4 May 2006.
[10] J. Corbett, et al, “Visible light diagnostics at SPEAR3”, SRI09, Melbourne, Australia, 2009.
[11] J. Byrd and S. De Santis, “Longitudinal injection transients in an electron storage ring”, PRST-AB, Vol. 4, 024401 (2001).